The present-day thermal state of Mars

Javier Ruiz [a,*], Valle López [b], James M. Dohm [c,d]

[a] Centro de Biología Molecular, CSIC-Universidad Autónoma de Madrid, 28049 Cantoblanco, Madrid, Spain
[b] Instituto Español de Oceanografía, Corazón de María 8, 28002 Madrid, Spain
[c] Department of Hydrology and Water Resources, University of Arizona, Tucson, 85721 AZ, USA
[d] The Museum, University of Tokyo, Tokyo 113-0033, Japan

Keywords:
Mars
Mars, Interior
Thermal histories

A B S T R A C T

The present-day thermal state of the martian interior is a very important issue for understanding the internal evolution of the planet. Here, in order to obtain an improved upper limit for the heat flow at the north polar region, we use the lower limit of the effective elastic thickness of the lithosphere loaded by the north polar cap, crustal heat-producing elements (HPE) abundances based on martian geochemistry, and a temperature-dependent thermal conductivity for the upper mantle. We also perform similar calculations for the south polar region, although uncertainties in lithospheric flexure make the results less robust. Our results show that the present-day surface and sublithospheric heat flows cannot be higher than 19 and 12 mW m^{-2}, respectively, in the north polar region, and similar values might be representative of the south polar region (although with a somewhat higher surface heat flow due to the radioactive contribution from a thicker crust). These values, if representative of martian averages, do not necessarily imply sub-chondritic HPE bulk abundances for Mars (as previously suggested), since (1) chondritic composition models produce a present-day total heat power equivalent to an average surface heat flow of 14–22 mW m^{-2} and (2) some convective models obtain similar heat flows for the present time. Regions of low heat flow may even have existed during the last billions of years, in accordance with several surface heat flow estimates of ~20 mW m^{-2} or less for terrains loaded during Hesperian or Amazonian times. On the other hand, there are some evidences suggesting the current existence of regions of enhanced heat flow, and therefore average heat flows could be higher than those obtained for the north (and maybe the south) polar region.

1. Introduction

Knowledge of the surface heat flow is very important for understanding the thermal and geologic evolution of a planetary body. There are not direct measurements for Mars, but heat flows have been deduced for diverse martian regions from the effective elastic thickness of the lithosphere (Solomon and Head, 1990; Anderson and Grimm, 1998; Zuber et al., 2000; Nimmo, 2002; Kiefer, 2004; McGovern et al., 2002, 2004; Grott et al., 2005; Ruiz et al., 2006, 2008; Kronberg et al., 2007; Ruiz, 2009; Dohm et al., 2009a; Ritzer and Hauck, 2009) or from the depth to the brittle–ductile transition beneath large thrust faults (Schultz and Watters, 2001; Grott et al., 2007; Ruiz et al., 2008, 2009). So deduced heat flows are valid for the time when the lithosphere was loaded or faulted, permitting us to delineate, in a first approximation, the thermal evolution of the planet (McGovern et al., 2002, 2004; Montesi and Zuber, 2003).

Given the lack of large scale tectonic activity at the present time, the possibility of using effective elastic thicknesses for estimating the present-day thermal state of this planet seems restricted to the polar regions, where loading by ice caps is a recent phenomenon, estimated to be a few million years old (Laskar et al., 2002; Phillips et al., 2008). Through the modeling of the deflection of the topography beneath the north polar cap due to ice loading, Phillips et al. (2008) found a lower limit of 300 km for the effective elastic thickness of the lithosphere at the north polar region. For the south polar region, Phillips et al. (2008) suggested a lower limit of 275–300 km for the effective elastic thickness, although the topographic evidences for this case are more uncertain. Effective elastic thicknesses around or higher than 300 km are clearly higher than any previously published value for Mars (e.g., McGovern et al., 2004). This could indicate that Mars is dead in a geodynamical sense (Grott, 2008).

On the other hand, Wieczorek (2008) obtained a best fit of 161 km for the effective elastic thickness of the south polar region through gravity/topography admittance modeling. However, this

author found that any value higher than 110 km can fit the observed admittance. A value of ~100 km or higher is similar to the effective elastic thicknesses obtained for the Hesperian/Amazonian-aged Valles Marineris region (McGovern et al., 2004), although the estimate for the south polar region is a lower limit. On the other hand, effective elastic thickness estimates for Amazonian-aged regions are usually lower than 100 km (McGovern et al., 2004; Belleguic et al., 2005), although these estimates were performed for volcanic regions, which could be hotter than average.

Phillips et al. (2008) estimated heat flows following the strength envelope procedure (McNutt, 1984) coupled with temperature profiles and crustal heat production rates deduced from the thermal history models of Hauck and Phillips (2002), obtaining surface and mantle heat flows of 25 and 17 mW m^{-2}, respectively. These results are very similar to those obtained by the nominal model of Hauck and Phillips (2002), and Phillips et al. (2008) conclude that, since the result for the north polar region is an upper limit, heat-producing elements (HPE) abundances for Mars are probably sub-chondritic (this conclusion was basically unchanged when a non-steady-state loading response was considered by these authors). In this sense, Grott and Breuer (2009a) found that thermal history models consistent with an average effective elastic thickness of at least 300 km require either sub-chondritic HPE abundances or a high fractionation of HPE in the crust and a dry mantle rheology. An alternative explanation is a spatially heterogeneous heat flow on Mars, which could naturally arise from mantle convection (Grott and Breuer, 2009a; Kiefer and Li, 2009).

The conclusions of Phillips et al. (2008) rely on HPE distributions and temperature profiles derived from thermal history models, and somewhat on the assumed mantle thermal conductivity (4 W m^{-1} K^{-1}), which is high for the lithospheric mantle. Here we derive a more robust calculation of upper limits for the surface and sublithospheric heat flow at both polar regions by using a HPE distribution based on geochemical considerations and more realistic thermal conductivities, including a temperature-dependent thermal conductivity for the lithospheric mantle; this procedure has the advantage of making the results independent of any specific thermal history model. We also discuss the implications of our results for the thermal history of Mars, as well as some possible evidences of regional variations in the current thermal state of the lithosphere.

2. Temperature at the base of the lithosphere

The effective elastic thickness of the lithosphere, which is a measure of the total strength of the lithosphere, can be converted to heat flow following the equivalent strength envelope procedure described by McNutt (1984). This methodology is based on the condition that the bending moment of the mechanical lithosphere must be equal to the bending moment of the equivalent elastic layer of thickness T_e. The link between the mechanical structure and heat flow comes from the dependence of the ductile strength on temperature.

If lithospheric flexure is small, then it can be neglected and T_e is equal to the depth to the base of the mechanical lithosphere, L, which is defined as the depth at which the ductile strength reaches a low value and below which there are no further significant increases in strength. The base of the mechanical lithosphere can be defined, therefore, as the depth to an isotherm given by

$$T_L = \frac{Q}{R \ln\left[\frac{A(\sigma_1-\sigma_3)_L^n}{\dot{\varepsilon}}\right]}, \tag{1}$$

where Q is the activation energy for creep, R (=8.31447 J mol^{-1} K^{-1}) is the gas constant, A and n are laboratory-determined constants, $(\sigma_1-\sigma_3)_L$ is the strength level defining the base of the mechanical lithosphere, and $\dot{\varepsilon}$ is the strain rate. The surface, subcrustal and sublithospheric heat flows can then be calculated by finding the temperature profile that fits the isotherm given by Eq. (1) at a depth equal to T_e. Surface heat flow decreases with topography curvature (McNutt, 1984; Solomon and Head, 1990), and therefore assuming no lithosphere flexure gives an upper limit to the heat flow. This is sufficient for the purposes of this work, as Phillips et al. (2008) did not determine a lower limit for lithospheric flexure.

We calculate the temperature defining the base of the mechanical lithosphere by using the flow law of dry olivine (Chopra and Paterson, 1984): Q = 535 kJ mol^{-1}, A = 28840 MPa^{-n} s^{-1}, and n = 3.6. For $(\sigma_1-\sigma_3)_L$ we use a value of 10 MPa, which is considered appropriate for the low gravity of Mars (see Ruiz et al., 2006), although the exact selected value does not produce significant changes in the calculations due to the exponential dependence of ductile strength on temperature. A strain rate of 10^{-14} s^{-1} is used in the calculations, which corresponds to an estimated age of ~5 Ma for the load by the north polar cap (Phillips et al., 2008). So, T_L = 1267 K is obtained. The use of a weaker wet olivine rheology would reduce both the temperature at the base of the lithosphere and the surface heat flow. For example, for the wet Anita Bay dunite (Chopra and Paterson, 1984) T_L = 1087 K, which would imply a reduction of less than 10% of the surface heat flow obtained in all the cases analyzed in the present work (see Sections 4 and 5).

3. Temperature profiles

We calculate thermal profiles for both north and south polar regions by considering a three layer model differencing between polar cap (not included in the lithosphere), crust and mantle lithosphere.

Polar caps are assumed to be composed of water–ice. The thermal conductivity of cold water–ice is high, and the presence of rocks or other ices (e.g., CO_2) would reduce the bulk thermal conductivity, and hence the calculated heat flow. For this reason, non-water–ice components are not taken into account in our upper-limit calculation. The thermal conductivity of water–ice is strongly temperature-dependent, and therefore the temperature profile in the polar cap is given by

$$T_{pcb} = T_s \exp\left(\frac{F b_{pc}}{k_0}\right), \tag{2}$$

where T_s is the surface temperature, F is the surface heat flow (equal to the heat flow reaching the polar cap from below), b_{pc} is the thickness of the polar cap, and k_0 = 621 W m^{-1} (Petrenko and Whitworth, 1999). Here we use T_s = 155 K and b_{pc} = 2 km as representatives for the martian polar regions (Plaut et al., 2007; Phillips et al., 2008; Wieczorek, 2008). Subsurface temperatures might be higher than those expected for a steady-state thermal profile, because cooler surface conditions related to obliquity and insolation changes implied in the growth of the polar caps (Laskar et al., 2002) would have a relatively limited downward propagation in a few million years; this would reduce the surface heat flow, reinforcing the robustness of the upper limits calculated in this work.

For the crust, homogeneously distributed radioactive heat sources and a constant thermal conductivity are assumed. So, the temperature at the base of the crust is given by

$$T_{cb} = T_{pcb} + \frac{F b_c}{k_c} - \frac{H_c b_c^2}{2k_c}, \tag{3}$$

where T_{pcb} is the surface temperature at the base of the polar cap, b_c is the thickness of the crust, k_c is the thermal conductivity of the crust, and H_c is the crustal volumetric heat production rate.

Crustal models for Mars (Neumann et al., 2004, 2008) indicate that the crust at the north polar region is typically ~15–25 km

thinner than the average martian crust. Wieczorek and Zuber (2004) have constrained the average martian crust to be between 38 and 62 km through simultaneously considering several geophysical and geochemical arguments, although 45 km is a reasonable lower limit for the nominal crustal density of 2900 kg m^{-3} (Neumann et al., 2004; Ruiz et al., 2008, 2009). So, the local crustal thicknesses at the north polar region would most likely be between ~20 and ~50 km. Similarly, the crust at the south polar region is ~15 km thicker than the average crust, implying a local crustal thickness between ~60 and ~80 km.

We use $k_c = 2.5$ W m^{-1} K^{-1} for the whole crust. The crustal thermal conductivity should be ~2 W m^{-1} K^{-1} if the martian crust is mostly basaltic (e.g., Clifford, 1993; Grott et al., 2005). The upper kilometers of the crust could be enriched in water ice, which would increase the thermal conductivity; Clifford (1993), for example, considers that the martian cryosphere would have an average thermal conductivity of ~3 W m^{-1} K^{-1}. However, crustal rock porosity and the thickness of a liquid water- or water–ice-enriched crust are poorly known. A value of 2.5 W m^{-1} K^{-1} is likely somewhat high for the average martian crust: this value is therefore useful for estimating an upper limit for the heat flow. If we use $k_c = 2$ W m^{-1} K^{-1}, the obtained heat flow is reduced less than 1 mW m^{-2} with respect to the results for the north polar region presented in Section 4; even for the south polar region and low effective elastic thickness, the reduction in surface heat flow is less than 15% with respect to the values obtained in Section 5.

For calculating the present-day crustal volumetric heating rate, we use potassium, thorium, and uranium abundances of 3740, 0.70, and 0.18 ppm respectively, which are average values estimated for the crust of Mars by the review of Taylor and McLennan (2009). These values are higher than average surface K and Th abundances deduced from Mars Odyssey GRS measurement (Taylor et al., 2006), but only slightly higher than a more recent refinement (correcting for water content) of the GRS data (Hahn and McLennan, 2008). The used values are useful for our purpose, since the obtained surface heat flow increases with the increasing of HPE in the crust (Ruiz et al., 2006). In the calculations we use a nominal crustal density of 2900 kg m^{-3} and decay constants from Van Schmus (1995), obtaining a volumetric heat production rate of 0.142 μW m^{-3} (or equivalently, a heat production rate by mass unity of 4.91×10^{-5} μW kg^{-1}).

The thermal conductivity of olivine, the mineral considered to dominate ductile deformation in lithospheric mantle rocks, exhibits a strong temperature-dependence. Here we use the expression (McKenzie et al., 2005)

$$k_m = \frac{a}{1 + c(T - 273)} + \sum_{i=0}^{3} d_i T^i, \tag{4}$$

where $a = 5.3$, $c = 0.0015$, $d_0 = 1.753 \times 10^{-2}$, $d_1 = -1.0364 \times 10^{-4}$, $d_2 = 2.2451 \times 10^{-7}$ and $d_3 = -3.4071 \times 10^{-11}$, for calculating an upper limit for the thermal conductivity of olivine as a function of temperature. Results obtained from Eq. (4) are similar to those of Hofmeister (1999) for forsterite olivine. The thermal conductivity of some silicate minerals (including olivine) somewhat decreases with the increasing of the proportion of iron (Hofmeister, 1999). The martian mantle is considered to be iron-rich (e.g., Halliday et al., 2001), and for this reason Eq. (4) gives an upper limit to the thermal conductivity of the mantle lithosphere of Mars.

We calculate the temperature profile across the lithospheric mantle by integration, from $z = b_c$ to L, of

$$dT = \frac{F_{cb} - H_m(z - b_c)}{k_m(T)} dz, \tag{5}$$

where $F_{cb} = F - H_c b_c$ is the heat flow at the base of the crust, and H_m is the volumetric heat production rate of the lithospheric mantle. The value of H_m is poorly constrained. Here we use $H_m = 0.1 H_c$, based on a ratio between crustal and primitive mantle HPE abundances higher than ~10 for Mars (Taylor and McLennan, 2009); this value represents a reasonable upper limit for H_m (melt extraction would reduce mantle HPE abundances), which in turn results in an upper limit to the obtained surface heat flow.

The surface heat flow is obtained by simultaneously solving Eqs. (2)–(5).

4. Heat flows in the north polar region

Fig. 1 shows the surface heat flow for $T_e = 300$ km as a function of the thickness of the crust in the north polar region. The upper limit obtained for the surface heat flow is 17–19 mW m^{-2}, depending on crustal thickness. Our values are lower than those of Phillips et al. (2008). Thus, a more restrictive upper limit, which does not depend on any pre-defined thermal history model, is imposed to the present-day heat flow of Mars in this region. Without lithospheric heat sources, the surface heat flow equals the sublithospheric heat flow. Therefore, an independent upper limit for the sublithospheric heat flow (essentially the heat flow from the deep planetary interior) can be estimated by assuming $H_c = 0$ and $H_m = 0$. This upper limit, which is 11–12 mW m^{-2} depending on the crustal thickness, is also shown in Fig. 1. Fig. 2 shows that subcrustal and sublithospheric heat flows obtained by including lithospheric heat sources are 11–14 and 8–10 mW m^{-2}, respectively, for $T_e = 300$ km. In this figure it is also observed that both the subcrustal and the sublithospheric heat flow decrease with the increasing of the crustal thickness, because the larger fraction of heat sources placed in a thicker crust.

Surface heat flows of ~20 mW m^{-2} or less have been previously proposed, based on estimates of the effective elastic thickness, for the Amazonian Tharsis region, the Hesperian/Amazonian Valles Marineris regions (Zuber et al., 2000; McGovern et al., 2004), and the Noachian- or Hesperian-loaded Isidis Planitia (Ritzer and Hauck, 2009). For example, the estimates for Amazonian terrains are all consistent with a surface heat flow between 13 and 24 mW m^{-2} (McGovern et al., 2004; Li and Kiefer, 2007). The effective elastic thicknesses obtained for these regions are clearly lower than that deduced for the north polar region, although it must be noted that for a given value of T_e the obtained heat flow decreases with the increasing of the curvature of the topography of the equivalent elastic plate (McNutt, 1984; Solomon and Head, 1990). Those calculations used a high mantle thermal conductivity of 4 W m^{-1} K^{-1} and no lithospheric heat sources. The use of a high mantle thermal conductivity increases the obtained heat flow (see Eqs. (3) and (5)). The existence

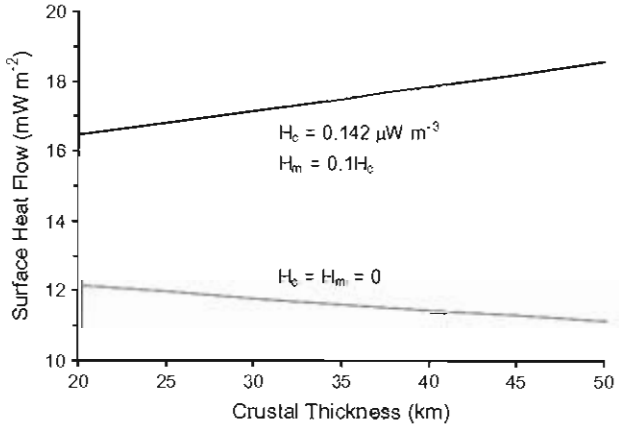

Fig. 1. Surface heat flow in the north polar region as a function of crustal thickness, calculated for $T_e = 300$ km and the cases including and not including lithospheric heat sources.

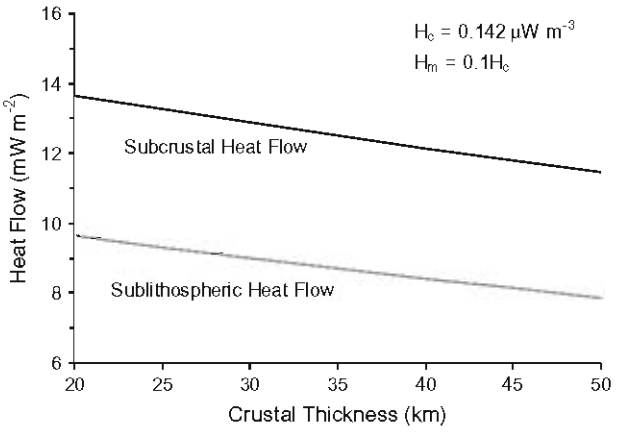

Fig. 2. Subcrustal and sublithospheric heat flow in the north polar region, as a function of crustal thickness, obtained for T_e = 300 km and the case including lithospheric heat sources.

of lithospheric heat sources implies a thermal profile between the surface and lithosphere base hotter than for the case without heat sources; this in turn gives a steeper near surface thermal gradient and a higher surface heat flow. Conversely, not taking into account lithospheric heat sources decreases the obtained surface heat flow. The above cited estimates of low heat flows for the Amazonian are therefore not totally comparable with our values, but they suggest that the present-day heat flow in the north polar region could not be much lower than those characterizing some regions during a substantial part of the martian history (although estimates for other Hesperian or Hesperian/Amazonian regions give higher heat flows; e.g., McGovern et al., 2004).

Thermal history models for Mars usually predict present-day average surface heat flows between 20 and 30 mW m^{-2} (e.g., Nimmo and Stevenson, 2000; Spohn et al., 2001; Hauck and Phillips, 2002; Arkani-Hamed, 2005; Grott and Breuer, 2009b). Schumacher and Breuer (2007) obtained a mantle heat flow (under the stagnant lid) of ~12 mW m^{-2} by considering convection with temperature-dependent mantle thermal conductivity. These authors do not give surface heat flow, but from their heat production rates (also based on chondritic HPE abundances), enrichment factors, and crustal and stagnant lid thicknesses, an average heat flow of 18–22 mW m^{-2} is obtained. The thermal history models of Grott and Breuer (2009a) are consistent with T_e = 300 km (for a not flexed lithosphere) for present-day surface heat flows of 11–20 and 14–20 mW m^{-2} for mantle convection with wet and dry rheology, respectively. (Noteworthy, water abundance, and hence rheology, in the deep and convective mantle is not necessarily the same as in the lithospheric mantle.) These values are consistent with our results, but the models of Grott and Breuer (2009a) require some degree of sub-chondritic HPE abundances for an upper limit of 19 mW m^{-2} for the surface heat flow. In turn, the thermal models by Grott and Breuer (2009b), which include a crustal HPE distribution dependent on crustal thickness and location and a wet convective mantle, find present-day average surface and sublithospheric heat flows of 21 and 14.5 mW m^{-2}, respectively; according to this model, a sublithospheric heat flow of ~9 mW m^{-2}, consistent with T_e = 300 km at the north polar region and our results considering lithospheric heat sources, require a reduction of HPE abundances with respect to the chondritic composition model of Wänke and Dreibus (1988). On the other hand, the models of steady-state convection for the present-day Mars of Li and Kiefer (2007), which include plume melting and chondritic HPE abundances, find surface heat flows under 20 mW m^{-2}, in accordance with our results.

Total radioactive heat power deduced from bulk composition models for Mars can be converted to an equivalent average surface heat flow. This is 14 and 22 mW m^{-2} (see Table 1) for, respectively, the bulk composition models of Wänke and Dreibus (1988) and Lodders and Fegley (1997). These models include chondritic HPE abundances, adjusted with SNC geochemistry, which differ in potassium abundance. The upper limit for the surface heat flow deduced for the north polar region is between these values.

Summarizing, if the present-day heat flow in the north polar region is representative of martian averages (although the effect of variations in crustal thickness on HPE distribution must be taken into account), then our results can be interpreted in two alternative ways:

(1) Martian HPE abundances are chondritic, mantle convection removes roughly as much heat as is radioactively generated, and the contribution of secular cooling to the present-day heat flow is less than predicted by the majority of thermal history models.
(2) Martian HPE bulk abundances are lower than predicted by geochemical models, and secular cooling could have a non-negligible contribution to the present-day heat flow.

5. Heat flows in the south polar region

The effective elastic thickness of the lithosphere of the south polar region is higher than 110 km (according to gravity/topography admittance modeling; Wieczorek, 2008, p. 515), and could be higher than 275 km (if the evidences of lithospheric flexure are correct; see Phillips et al., 2008). Crustal thicknesses typical of the southern hemisphere of Mars could permit the mechanical decoupling between the crust and lithospheric mantle, depending on temperature profile and crustal rheology. For a given effective elastic thickness, the obtained heat flow is in that case lower than if the crust is mechanically welded to the lithospheric mantle (Ruiz et al., 2008). It is not clear if a dry or wet rheology is pertinent for the martian crust at the present time, but a dry diabase rheology (Mackwell et al., 1998) would preclude crust/mantle decoupling for the values of crustal thickness and effective elastic thickness deduced for the south polar region of Mars. Crust/mantle decoupling is therefore not considered in our upper-limit calculations presented in this section.

Fig. 3 shows surface heat flows for the south polar region, as a function of the effective elastic thickness, for crustal thicknesses of 60 and 80 km. Fig. 3 also shows heat flows for zero lithospheric heat sources, a case which gives a generous upper limit to the sublithospheric heat flow. Surface and deep mantle heat flows may be as high as 32 and 26 mW m^{-2}, respectively (for T_e = 110 km), although they might be lower than 20–21 mW m^{-2} and 11–12 mW m^{-2}, respectively (for T_e > 275 km), for the south polar region. The latter values are similar to those obtained for the north polar region.

Table 1
HPE abundances for Mars.

	Wänke and Dreibus (1988)	Lodders and Fegley (1997)
Bulk silicate[a] abundance		
K (ppm)	305	920
Th (ppb)	56	56
U (ppb)	16	16
Silicate fraction[b]	0.7937	0.783
Equivalent heat flow (mW m^{-2})[c]	14.3	21.9

[a] Crust plus mantle.
[b] Total silicate mass/total mass of Mars.
[c] Equivalent surface heat flow is calculated from martian mass and radius of Sohl et al. (2005), and decay constant of Van Schmus (1995).

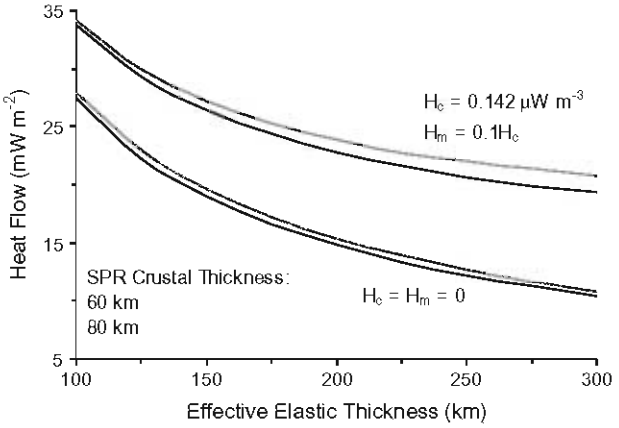

Fig. 3. Surface heat flow in the south polar region, as a function of the effective elastic thickness, calculated for crustal thicknesses of 60 and 80 km and the cases including and not including lithospheric heat sources.

Fig. 4 shows surface and sublithospheric heat flows for the south polar region as a function of the effective elastic thickness, calculated for b_c = 60 km and including lithospheric heat sources, compared with the equivalent heat flows for the north polar region, b_c = 25 km, and T_e = 300 km; crustal thicknesses have been selected from an average thickness of 45 km for the martian crust, corresponding to the nominal model of Neumann et al. (2004). If T_e > 275 km in the south polar region, then the present-day sublithospheric heat flow may be similar, ~8–9 mW m^{-2}, under both polar regions, although there would be a certain difference in surface heat flow because the higher crustal thickness in the south polar region (however, for a thicker crust the effect of a higher radioactive contribution to the surface heat flow is partly compensated by the lower thermal conductivity of the crust).

Summarizing, results for the south polar region are less restrictive than those obtained for the north polar region, due to uncertainties in lithospheric deflection. The surface and sublithospheric heat flow might be similarly low in both regions, but it is not sure.

6. Regional variations in the thermal state of the lithosphere

The present-day heat flow at both polar regions might not be representative of martian averages. For example, convective models by Kiefer and Li (2009) predict present-day mantle heat flow variations higher than a factor 2. In this section we discuss evidences of possible local variations in the current thermal state of the martian lithosphere.

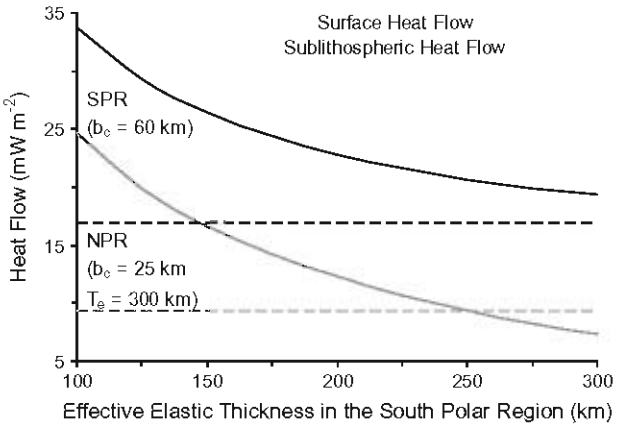

Fig. 4. Surface and sublithospheric heat flow in the south polar region (SPR) as a function of the effective elastic thickness and calculated for a crustal thickness of 60 km (solid curves), compared with the equivalent ones for the north polar region (NPR), calculated for T_e = 300 km and a crustal thickness of 25 km (horizontal dashed lines).

The possibility of a currently dead Mars is challenged by published geologic information that indicates geologic and hydrologic activity into the Late Amazonian epoch. Indeed, endogenic-driven activity for at least parts of Mars is strongly suggested by a collection of geologic, hydrologic, topographic, chemical, and elemental evidences obtained by Viking, Mars Global Surveyor, Mars Odyssey, Mars Exploration Rovers, and Mars Express missions (see Dohm et al., 2008 and references therein). The evidence is especially highlighted in the Tharsis/Elysium corridor region (Dohm et al., 2008), which includes (also see Table 2): (1) stratigraphically young rock materials such as pristine lava flows with few, if any, superposed impact craters; (2) tectonic features that cut stratigraphically young materials; (3) features with possible aqueous origin such as structurally-controlled channels that dissect stratigraphically young materials and anastomosing-patterned slope streaks on hillslopes; and (4) spatially varying elemental abundances for such elements as hydrogen (H) and chlorine (Cl) recorded in rock materials up to 1/3 m deep. Therefore, an elevated heat flow for parts of the Tharsis and Elysium volcanic provinces, as well as the Tharsis/Elysium corridor region, is suggested by stratigraphic relations among rock materials and structures, as well as crater statistics.

Another line of evidence comes from the discovery of diffuse methane plumes arising from a wide zone including Syrtis Major, Nili Fossae and eastern Arabia Terra regions (Mumma et al., 2009). The concurrence in this area of the Syrtis Major volcanic structure, as well as the fracture system of Nili Fossae, suggest an endogenic origin for the methane plumes, although a biological origin has also been proposed for the origin of martian methane (e.g., Krasnopolsky, 2006). These plumes may therefore be an indication of locally enhanced endogenic activity.

A completely different line of evidence could also support the spatial association among an area of elevated heat flow and the source area of the methane plumes. Indeed, the two global paleoshorelines proposed for Mars (Parker et al., 1993; Clifford and Parker, 2001), named Deuteronilus and Arabia shorelines, have a higher large-scale elevation at the northern plains adjacent to the Syrtis Major/Nili Fossae region than in other regions (Fig. 5; see also Figs. 5 and 10 of Carr and Head (2003)). Deviations of equipotentiality along martian paleoshorelines could be caused by modification of the original topography due to thermal isostasy related to different thermal histories between the regions transected by these paleoshorelines (Ruiz, 2003; Ruiz et al., 2004).

The paleoshoreline hypothesis is controversial, due to different interpretations proposed for the putative coastal features (see Clifford and Parker, 2001; Ghatan and Zimbelman, 2006), but there is a strong support for a distinctive geochemical signature, consistent with aqueous activity and the paleoshoreline demarcations, at the northern plains of Mars (Dohm et al., 2009b). Moreover, the present-day topography of the Deuteronilus shoreline is acceptably close to an equipotential surface (Head et al., 1999; Carr and Head, 2003), and the influence of ocean desiccation on rotation axis and geoid shape could explain the large-scale trends of departure from equipotential surfaces of both Deuteronilus and Arabia shorelines (Perron et al., 2007). However, the portions of both putative shorelines closer to the methane source region are hundreds of meters more elevated than predicted when the effects of ocean desiccation are taken into account (see Fig. 1b of Perron et al. (2007)). Thus, the concurrence at a same region of volcanic and tectonized terrains, methane plumes, and more elevated than average possible paleoshorelines, strongly suggests a region of enhanced heat flow.

Table 2
Geologic activity within the Tharsis/Elysium corridor regions during the Amazonian Period (EA: Early Amazonian, MA: Middle Amazonian, LA: Late Amazonian) (see Dohm et al., 2008 and references therein). Note that the commencement and/or end of activity of the listed features are not exactly constrained by the commencement and/or end of the periods.

Activity	EA	MA	LA
Late-stage development of Tharsis	→	→	→
Development of Syria Planum, a corona-like feature	→		
Elysium rise development	→	→	→
Late-stage Tharsis Montes and Olympus Mons development	→		
Emplacement of lavas centered at Tharsis Montes, Alba Patera, and Syria Planum	→		
Continued change from widespread Tharsis magmatic-tectonic activity initiated during the Late Hesperian to centralized volcanism to forge the giant shield volcanoes of Tharsis Montes, Olympus Mons, and Alba Patera	→		
Significant waning of tectonism in the western hemisphere except at Alba Patera	→		
Continued construction of Olympus Mons	→	→	→
Late-stage volcanic activity at Elysium rise	→	→	→
Late-stage volcanic activity at Tharsis Montes, which includes emplacement of the aureole deposits	→	→	→
Emplacement of the Medusae Fossae materials; materials could be ash-flow tuffs, ancient polar deposits, or pyroclastic and eolian materials	→	→	→
Magmatic–tectonic activity in a region south of Ascraeus	→	→	→
Local tectonism associated with some of the large shield volcanoes including Tharsis Montes	→	→	→
Emplacement of the aureole deposits, interpreted to be the result of late-stage glaciation and interaction between ice and lavas		→	→

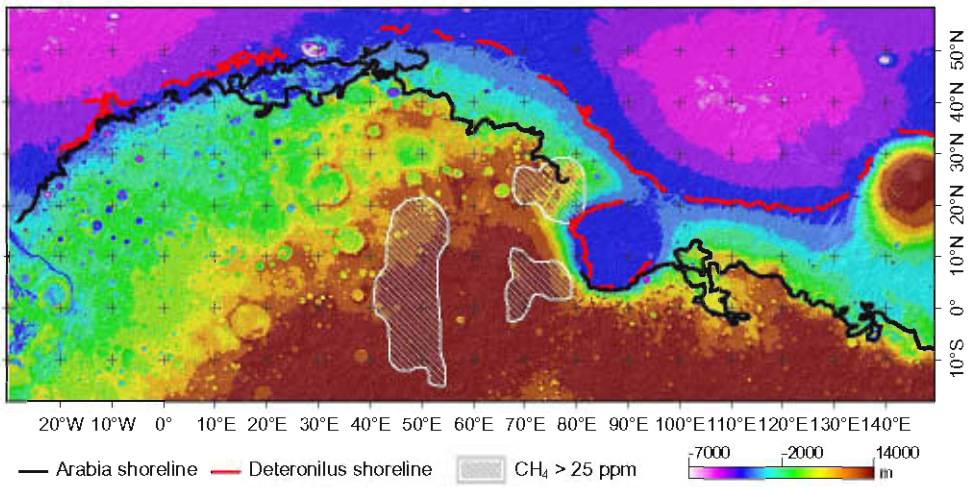

Fig. 5. Spatial association of the source area of methane plumes (Mumma et al., 2009) and high large-scale elevation of putative ocean paleoshorelines proposed for Mars (after Clifford and Parker, 2001). The highest elevation of the Deuteronilus shoreline coincides with its maximum proximity to the methane source area. The Arabia shoreline is also less elevated to the west of the methane source area, although not to the east; however, this zone is close to the volcanic area of Elysium.

The average heat flow of Mars might, therefore, be higher than the value obtained for the north polar region.

7. Conclusions

Our results show that the present-day surface heat flow at the north polar region is 19 mW m^{-2} at most. Similarly, the heat flow arising to the lithosphere from the deep mantle cannot be higher than 12 mW m^{-2}. Heat flows at the south polar region might be similar to those of the north polar region, but it is not sure due to the uncertainty in estimating lithospheric deflection. The global relevance of these values is not clear, but there are some evidences suggesting the existence of regions of comparatively elevated heat flow, such as the Tharsis/Elysium corridor and the methane source region. On the other hand, even if heat flows obtained for the north (and maybe south) polar region are representative of martian averages, our results are not necessarily incompatible with chondritic HPE abundances. Indeed, the total radioactive heat power deduced from chondritic models of bulk composition of Mars is equivalent to an average surface heat flow of 14–22 mW m^{-2}, and some convective models obtain a present-day surface heat flow lower than 20 mW m^{-2}. Moreover, there are several previous estimates of surface heat flow of ~20 mW m^{-2} or less for terrains loaded during the Hesperian or Amazonian Periods. Maybe, regions of low surface heat flow have been common during the last two or three billions of years. This possibility and its implication for the thermal history models of Mars require further careful investigation.

Acknowledgments

We thank the useful comments and suggestions of two anonymous reviewers, and the encouragement of Ricardo Amils. J.R. work was supported by a contract Juan de la Cierva for Earth Sciences, co-financed from the Ministerio de Ciencia e Innovación of Spain and the European Social Fund. This paper is dedicated to the memory of Carisio Fernández, an enthusiast of Mars.

References

Anderson, S., Grimm, R.E., 1998. Rift processes at the Valles Marineris, Mars: Constraints from gravity on necking and rate-depending strength evolution. J. Geophys. Res. 103, 11113–11124.

Arkani-Hamed, J., 2005. Magnetic crust of Mars. J. Geophys. Res. 110. E08005. doi:10.1029/2004JE002397.

Belleguic, V., Lognonné, P., Wieczorek, M., 2005. Constraints on the martian lithosphere from gravity and topography data. J. Geophys. Res. 110. E11005. doi:10.1029/2005JE002437.

Carr, M.H., Head, J.W., 2003. Oceans on Mars: An assessment of the observational evidence and possible fate. J. Geophys. Res. 108 (E5), 5042. doi:10.1029/2002JE001963.
Chopra, P.N., Paterson, M.S., 1984. The role of water in the deformation of dunite. J. Geophys. Res. 89, 7861–7876.
Clifford, S.M., 1993. A model for the hydrologic and climatic behaviour of water on Mars. J. Geophys. Res. 98, 10973–11016.
Clifford, S.M., Parker, T.J., 2001. The evolution of the martian hydrosphere: Implications for the fate of a primordial ocean and the current state of the northern plains. Icarus 154, 40–79.
Dohm, J.M., and 21 colleagues, 2008. Recent geological and hydrological activity on Mars: The Tharsis/Elysium corridor. Planet. Space Sci. 56, 985–1013.
Dohm, J.M., and 13 colleagues, 2009a. Claritas rise, Mars: Pre-Tharsis Magmatism? J. Volcanol. Geotherm. Res. doi:10.1016/j.jvolgeores.2009.03.012.
Dohm, J.M., and 20 colleagues, 2009b. GRS evidence and the possibility of paleooceans on Mars. Planet. Space Sci. 57, 664–684.
Ghatan, G.J., Zimbelman, J.R., 2006. Paucity of candidate coastal constructional landforms along proposed shorelines on Mars: Implications for a northern lowlands-filling ocean. Icarus 185, 171–196.
Grott, M., 2008. Is Mars geodynamically dead? Science 320, 1171–1172.
Grott, M., Breuer, D., 2009a. Implications of large elastic thicknesses for the composition and current thermal state of Mars. Icarus 201, 540–548.
Grott, M., Breuer, D., 2009b. On the spatial variability of the martian elastic lithosphere thickness: Evidence for mantle plumes? J. Geophys. Res., in press, doi:10.1029/2009JE003456.
Grott, M., Hauber, E., Werner, S.C., Kronberg, P., Neukum, G., 2005. High heat flux on ancient Mars: Evidence from rift flank uplift at Coracis Fossae. Geophys. Res. Lett. 32. L21201. doi:10.1029/2005GL023894.
Grott, M., Hauber, E., Werner, S.C., Kronberg, P., Neukum, G., 2007. Mechanical modelling of thrust faults in the Thaumasia region, Mars, and implications for the Noachian heat flux. Icarus 186, 517–526.
Hahn, B.C., McLennan, S.M., 2008. Martian surface heat production and crustal heat flow from Mars Odyssey gamma-ray spectrometry. Proc. Lunar Sci. Conf. 39. Abstract 2032.
Halliday, A.N., Wänke, H., Birck, J.L., Clayton, R.N., 2001. The accretion, composition and early differentiation of Mars. Space Sci. Rev. 96, 197–230.
Hauck, S.A., Phillips, R.J., 2002. Thermal and crustal evolution of Mars. J. Geophys. Res. 107. doi:10.1029/2001JE001801.
Head, J.W., Hiesinger, H., Ivanov, M.A., Krelavshky, M.A., Pratt, S., Thomson, B.J., 1999. Possible ancient oceans on Mars: Evidence from Mars Orbiter Laser Altimeter Data. Science 286, 2134–2137.
Hofmeister, A.M., 1999. Mantle values of thermal conductivity and the geotherm from phonon lifetimes. Science 283, 1699–1706.
Kiefer, W.S., 2004. Gravity evidence for a extinct magma chamber beneath Syrtis Major, Marts: A look at the magmatic plumbing system. Earth Planet. Sci. Lett. 222, 349–361.
Kiefer, W.S., Li, Q., 2009. Mantle convection controls the observed lateral variations in lithospheric thickness on present-day Mars. Geophys. Res. Lett. 36. L18203. doi:10.1029/2009GL039827.
Krasnopolsky, V.A., 2006. Some problems related to the origin of methane on Mars. Icarus 180, 359–367.
Kronberg, P., Hauber, E., Grott, M., Werner, S.C., Schäfer, T., Gwinner, K., Giese, B., Masson, P., Neukum, G., 2007. Acheron Fossae, Mars: Tectonic rifting, volcanism, and implications for lithospheric thickness. J. Geophys. Res. 112. E04005. doi:10.1029/2002JE001854.
Laskar, J., Levrard, B., Mustard, J.F., 2002. Orbital forcing of the martian polar layered deposits. Nature 419, 375–377.
Li, Q., Kiefer, W.S., 2007. Mantle convection and magma production on present-day Mars: Effects of temperature-dependent rheology. Geophys. Res. Lett. 34. L16203. doi:10.1029/2007GL030544.
Lodders, K., Fegley, B., 1997. An oxygen isotope model for the composition of Mars. Icarus 126, 373–394.
Mackwell, S.J., Zimmerman, M.E., Kohlstedt, D.L., 1998. High-temperature deformation of dry diabase with application to tectonics on Venus. J. Geophys. Res. 103, 975–984.
McGovern, P.J., Solomon, S.C., Smith, D.E., Zuber, M.T., Simons, M., Wieczorek, M.A., Phillips, R.J., Neumann, G.A., Aharonson, O., Head, J.W., 2002. Localized gravity/topography admittance and correlation spectra on Mars: Implications for regional and global evolution. J. Geophys. Res. 107, 5136. doi:10.1029/2002JE001854.
McGovern, P.J., Solomon, S.C., Smith, D.E., Zuber, M.T., Simons, M., Wieczorek, M.A., Phillips, R.J., Neumann, G.A., Aharonson, O., Head, J.W., 2004. Correction to localized gravity/topography admittance and correlation spectra on Mars: Implications for regional and global evolution. J. Geophys. Res. 109. E07007. doi:10.1029/2004JE002286.
McKenzie, D., Jackson, J., Priestley, K., 2005. Thermal structure of oceanic and continental lithosphere. Earth Planet. Sci. Lett. 233, 337–349.
McNutt, M.K., 1984. Lithospheric flexure and thermal anomalies. J. Geophys. Res. 89, 11180–11194.
Montesi, L.G.J., Zuber, M.T., 2003. Clues to the lithospheric structure of martian from wrinkle ridge sets and localization instability. J. Geophys. Res. 108, 5048. doi:10.1029/2002JE001974.
Mumma, M.J., Villanueva, G.L., Novak, R.E., Hewagama, T., Bonev, B.P., DiSanti, M.A., Mandell, A.M., Smith, M.D., 2009. Strong release of methane on Mars in northern summer 2003. Science 323, 1041–1045.
Neumann, G.A., Zuber, M.T., Wieczorek, M.A., McGovern, P.J., Lemoine, F.G., Smith, D.E., 2004. The crustal structure of Mars from gravity and topography. J. Geophys. Res. 109. E08002. doi:10.1029/2004JE002262.
Neumann, G.A., Lemoine, F.G., Smith, D.E., Zuber, M.T., 2008. Marscrust3-A crustal thickness inversion from recent MRO gravity solutions. Proc. Lunar Sci. Conf. 39. Abstract 2167.
Nimmo, F., 2002. Admittance estimates of mean crustal thickness and density at the martian hemispheric dichotomy. J. Geophys. Res. 107, 5117. doi:10.1029/2000JE001488.
Nimmo, F., Stevenson, D.J., 2000. Influence of early plate tectonics on the thermal evolution and magnetic field of Mars. J. Geophys. Res. 105, 11969–11979.
Parker, T.J., Gorsline, D.S., Saunders, R.S., Pieri, D.C., Schneeberger, D.M., 1993. Coastal geomorphology of the martian northern plains. J. Geophys. Res. 98, 11061–11078.
Perron, J.T., Mitrovica, J.X., Manga, M., Matsuyama, I., Richards, M.A., 2007. Evidence for an ancient martian ocean in the topography of deformed shorelines. Nature 447, 840–843.
Petrenko, V.F., Whitworth, R.W., 1999. Physics of Ice. Oxford Univ. Press, Oxford. 366pp..
Phillips, R.J., and 26 colleagues, 2008. Mars north polar deposits: Stratigraphy, age, and geodynamical response. Science 320, 1182–1185.
Plaut, J.J., and 23 colleagues, 2007. Subsurface radar sounding of the south polar layered deposits of Mars. Science 316, 92–95.
Ritzer, J.A., Hauck, S.A., 2009. Lithospheric structure and tectonic at Isidis Planitia, Mars. Icarus 201, 528–539.
Ruiz, J., 2003. Amplitude of heat flow variations on Mars from possible shoreline topography. J. Geophys. Res. 108 (E5), 5122. doi:10.1029/2003JE002084.
Ruiz, J., 2009. The very early thermal state of Terra Cimmeria: Implications for magnetic carriers in the crust of Mars. Icarus. doi:10.1016/j.icarus.2009.05.021.
Ruiz, J., Fairén, A.G., Dohm, J.M., Tejero, R., 2004. Thermal isostacy and deformation of possible paleoshorelines on Mars. Planet. Space Sci. 52, 1297–1301.
Ruiz, J., McGovern, P.J., Tejero, R., 2006. The early thermal and magnetic state of the cratered highlands of Mars. Earth Planet. Sci. Lett. 241, 2–10.
Ruiz, J., Fernández, C., Gomez-Ortiz, D., Dohm, J.M., López, V., Tejero, R., 2008. Ancient heat flow, crustal thickness, and lithospheric mantle rheology in the Amenthes region, Mars. Earth Planet. Sci. Lett. 270, 1–12.
Ruiz, J., Williams, J.P., Dohm, J.M., Fernández, C., López, V., 2009. Ancient heat flows and crustal thickness at Warrego rise, Thaumasia Highlands, Mars: Implications for a stratified crust. Icarus. doi:10.1016/j.icarus.2009.05.008.
Schultz, R.A., Watters, T.R., 2001. Forward mechanical modeling of the Amenthes Rupes thrust fault on Mars. Geophys. Res. Lett. 28, 4659–4662.
Schumacher, S., Breuer, D., 2007. An alternative mechanism for recent volcanism on Mars. Geophys. Res. Lett. 34. L14202. doi:10.1029/2007GL030083.
Sohl, F., Schubert, G., Spohn, T., 2005. Geophysical constraints on the composition and structure of the martian interior. J. Geophys. Res. 110. E12008. doi:10.1029/2005JE002520.
Solomon, S.C., Head, J.W., 1990. Heterogeneities in the thickness of the elastic lithosphere of Mars: Constraints on heat flow and internal dynamics. J. Geophys. Res. 95, 11073–11083.
Spohn, T., Acuña, M.H., Breuer, D., Golombek, M., Greeley, R., Halliday, A., Hauber, E., Jaumann, R., Sohl, F., 2001. Geophysical constraints on the evolution of Mars. Space Sci. Rev. 96, 231–262.
Taylor, S.R., McLennan, S.M., 2009. Planetary Crusts: Their Composition, Origin and Evolution. Cambridge Univ. Press, Cambridge.
Taylor, G.J., and 22 colleagues, 2006. Bulk composition and early differentiation of Mars. J. Geophys. Res. 111, E03S10. doi:10.1029/2005JE002645 (Printed 112 (E3), 2007).
Van Schmus, W.R., 1995. Natural radioactivity of the crust and mantle. In: Ahrens, T.J. (Ed.), Global Earth Physics: A Handbook of Physical Constants. AGU Reference Shelf 1. American Geophysical Union, Washington, DC, pp. 283–291.
Wänke, H., Dreibus, G., 1988. Chemical composition and accretion history of terrestrial planets. Philos. Trans. R. Soc. Lond. A 325, 545–557.
Wieczorek, M.A., 2008. Constraints on the composition of the martian south polar cap from gravity and topography. Icarus 196, 506–517.
Wieczorek, M.A., Zuber, M.T., 2004. Thickness of the martian crust: Improved constraints from geoid-to-topography ratios. J. Geophys. Res. 109. E01009. doi:10.1029/2003JE002153.
Zuber, M.T., and 14 colleagues, 2000. Internal structure and early thermal evolution of Mars from Mars Global Surveyor. Science 287, 1788–1793.